I&EC research
Industrial & Engineering Chemistry Research

pubs.acs.org/IECR Article

Techno-Economic and Energy Assessment of the Pressure Swing Adsorption Process for CO_2 Capture from Flue Gas Using Shaped MOF MIL-160(Al): Bridging Experimental Results into Industrial Implementation

Mohsen Karimi,* Mohammad Shirzad, Rafael M. Siqueira, Alexandre Ferreira, José A. C. Silva, and Alírio E. Rodrigues

Cite This: *Ind. Eng. Chem. Res.* 2026, 65, 4633−4647 Read Online

ACCESS | Metrics & More | Article Recommendations | Supporting Information

ABSTRACT: This work provides an integrated techno-economic and energy assessment of vacuum pressure swing adsorption (VPSA) for postcombustion CO_2 capture, bridging laboratory-scale validation with industrial-scale design. The shaped MOF MIL-160(Al) was evaluated through 19 dynamic PSA experiments, which clarified the distinct roles of purge and rinse steps in determining the separation efficiency. The validated process model reliably captured cyclic steady-state dynamics and was extended to simulate 31 industrial VPSA configurations. The results demonstrated that as purge flow increased from 500 to 7.5×10^3 L/min, CO_2 purity reduced from 91% to 82%, but CO_2 recovery increased from 65% to 96%, which corresponds to an enhancement in energy consumption from 1589.2 to 1655 kWh. On the other hand, when rinse flow enhanced from 30×10^3 to 39×10^3 L/min, CO_2 purity increased from 82% to 89%, while CO_2 recovery reduced from 90% to 86% and energy consumption increased from 1573.5 to 1657.9 kWh. Techno-economic analysis estimated a total capital investment of \$18.89 M and an annualized capital expenditure (CapEx) of \$1.82 $M \cdot yr^{-1}$, with operating costs dominated by electricity consumption and, to a lesser extent, labor cost. Overall, the findings prove that industrially viable deployment of MIL-160(Al)-based VPSA requires a combined focus on plant equipment lifetime and process-level energy optimization, thereby providing a clear roadmap for translating experimental performance into large-scale CO_2 capture.

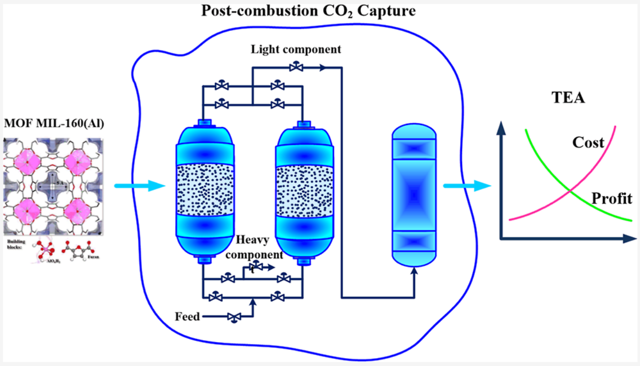

1. INTRODUCTION

The escalating global concern over climate change is predominantly driven by the sharp rise in atmospheric CO_2 concentrations, with global emissions having increased markedly over recent decades.[1,2] This upward trend is primarily attributed to the sustained and widespread combustion of fossil fuels—namely, coal, petroleum, and natural gas—which collectively account for approximately 86% of anthropogenic greenhouse gas emissions.[3,4] The remainder stems from land use changes, particularly deforestation, and industrial chemical processes.[5] In response to the growing environmental threats posed by elevated greenhouse gas levels, various national and international entities have implemented comprehensive mitigation frameworks.[6] Hence, projections of future greenhouse gas emissions are frequently framed within scenario analyses developed by authoritative bodies such as the International Energy Agency (IEA) and IPCC.[5,7] These models consistently indicate that to limit global warming to no more than 2 °C above preindustrial levels, it is imperative to reduce global anthropogenic CO_2 emissions to below 20 $GtCO_2$ annually by midcentury.[8] Moreover, achieving long-term climate stabilization will likely necessitate a transition toward near-zero emissions or even net-negative emissions by the latter part of the 21st century. However, among the key strategies under development, carbon capture and sequestration (CCS) has emerged as a critical solution for curbing CO_2 emissions associated with fossil-fuel-based energy systems. Nonetheless, the implementation of CCS faces substantial challenges, with CO_2 capture remaining one of the most pressing issues in the 21st century.[6,9,10] Notably, the capture stage is estimated to represent nearly two-thirds of the total cost of a full CCS system, thereby posing a major barrier to its large-scale deployment.[6] According to recent analyses,[11] the energy demand for

Received: November 28, 2025
Revised: February 9, 2026
Accepted: February 11, 2026
Published: February 19, 2026

ACS Publications

https://doi.org/10.1021/acs.iecr.5c04931

regeneration and the capital investment in capture-specific equipment are two principal cost drivers in postcombustion CO_2 capture technologies.

Despite the development of various CO_2 capture technologies for postcombustion applications,[12,13] lately, metal−organic frameworks (MOFs) have attracted growing attention for postcombustion CO_2 capture due to their tunable porosity, surface chemistry, and adsorption selectivity.[14,15] Nevertheless, their industrial deployment faces significant challenges, particularly due to their limited hydrothermal stability and reduced CO_2 uptake in humid environments.[16] Since water vapor is a major component of flue gas, the integration of moisture-sensitive MOFs into real-world systems remains problematic. However, in this way, plentiful MOFs have been introduced for CO_2 capture,[17,18] but only a limited number have undergone evaluation under realistic process conditions.[14,19,20] A primary constraint is the difficulty in synthesizing MOFs at scales sufficient for process-level testing, often limited to gram-scale quantities, and the synthesis cost is another main challenge of MOFs materials. On the other hand, the performance of cyclic adsorption systems for CO_2 capture is closely governed by both the properties of the adsorbent and the design of the operational cycle (e.g., PSA, VPSA, TSA).[20,21] Nevertheless, due to the intricate interactions among multiple process variables, identifying the optimal operating conditions to achieve targeted separation performance continues to pose a significant challenge.[20,22] This complexity is especially pronounced when using MOF sorbents, as their behavior under dynamic, multistep cycling is not yet fully understood.

On these grounds, several MOFs have been studied for the capture of CO_2 from flue gas through cyclic adsorption processes. For instance, Nikolaidis et al.[23] employed a two-stage P/VSA configuration incorporating Mg-MOF-74 and 13X, achieving CO_2 purities up to 95%. Ye et al.[24] reported enhanced CO_2/N_2 selectivity for HKUST-1 over MIL-101(Cr) under TSA conditions. Ben-Mansour et al.[25] highlighted the suitability of Mg-MOF-74 in heat-integrated PSA cycles, and CALF-20 was shown to achieve 95% CO_2 purity and 90% recovery under light-product pressurization.[26] It is worth noting that recently, MOF MIL-120(Al) has also been introduced as an appealing candidate for CO_2 capture from flue gas.[27] This adsorbent exhibited high CO_2 uptake (1.9 mmol g^{-1} at 0.1 bar, 298 K) with a logical isosteric heat of adsorption (−44 kJ mol^{-1}) and a rational synthesized cost which is interestingly water stable.[28,29] However, to our knowledge, the separation performance of MIL-120 through the cyclic adsorption processes (PSA, VPSA, TSA etc.) has not been reported yet.

Among the numerous efforts, which have explored water-stable MOFs using high-valence metal cations (e.g., Zr, Ti, Al, Fe, Cr),[30] recently the Al-based dicarboxylate MOF MIL-160(Al) has been introduced, which constructed from bioderived 2,5-FDCA (furan-2,5-dicarboxylic acid), exhibits exceptional hydrophilicity and stability, making it suitable for diverse sorption applications.[15,30] MIL-160(Al) features microporous channels (5−6 Å) formed by $AlO_4(OH)_2$ octahedra linked via 2,5-FDCA ligands, structurally analogous to CAU-10(Al).[30] Its scalable, green synthesis under ambient conditions achieves high space-time yields (>160 kg·day^{-1}·m^{-3}).[31] Also, it has already demonstrated a rational synthesize cost for industrial application,[32] and a better performance for CO_2 capture from flue gas than benchmark adsorbents, for instance zeolite 13X.[33] Furthermore, shaping into mechanically robust granules (crushing strength ∼10 N) via wet granulation with 5 wt % silica binder retains near-identical sorption performance to the powder form.[30] Accordingly, in this study, the shaped form MOF MIL-160(Al) has been studied for CO_2/N_2 separation from the lab-scale to the industrial scale concerning the postcombustion application.

1.1. Techno-Economic Assessment (TEA)

The fundamental objective of any chemical process is to ensure economic profitability; hence, a comprehensive understanding of process economics is indispensable in the process design and evaluation. Within this framework, process economics fulfills three principal roles: (i) enabling the comparison of alternative design strategies, (ii) guiding process optimization, and (iii) determining overall project profitability.[34]

A detailed cost assessment is particularly critical when evaluating different carbon mitigation pathways as it provides a quantitative basis for selecting the most financially viable option. Process variables, such as operating conditions and material selection, can exert a substantial influence on both flowsheet configuration and project economics, underscoring the need for rigorous optimization to maximize efficiency and minimize costs.[35] Moreover, economic feasibility must be verified at successive design stages to ensure that the project remains both technically and financially sustainable.[36,37]

In this regard, TEA provides a robust framework for quantitatively assessing the financial performance of adsorption-based systems. In the present study, the final annualized cost (FAC) is determined by integrating both capital expenditures (CapEx) and operating expenditures (OpEx).[34]

1.2. Research Objectives

In pursuit of CCS solutions, this study presents a comprehensive assessment of CO_2/N_2 separation using (vacuum) pressure swing adsorption ((V)PSA) for postcombustion applications, spanning lab-scale experiments to industrial-scale implementation. Initially, two dynamic breakthrough experiments were conducted and simulated to validate the accuracy of the developed model. Subsequently, to evaluate the interaction effects of purge and rinse flow rates, key operating variables governing separation performance, and to determine their optimal values, 19 lab-scale PSA experiments were performed using shaped MIL-160(Al) adsorbent. The experimental results were further supported by process simulations, highlighting conditions that maximized the performance.

In the next phase, an industrial-scale VPSA process was designed for the capture of CO_2 from flue gas. Employing a similar methodology, 31 distinct VPSA configurations were analyzed, with key performance indicators (KPIs) including CO_2 purity, recovery rate, productivity, and energy consumption—quantified for both lab- and industrial-scale systems. This systematic investigation revealed how variations in rinse and purge flow rates impact process efficiency at scale.

A detailed techno-economic assessment (TEA) was conducted to evaluate the economic feasibility of deploying MIL-160(Al)-based VPSA technology for industrial CO_2 capture. The analysis incorporated capital (CapEx) and operational (OpEx) expenditures, covering equipment sizing, energy requirements, and auxiliary infrastructure. Production costs were rigorously calculated under specified operating conditions, and sensitivity analyses identified critical factors (e.g., electricity price and plant lifetime) affecting cost-effectiveness. These findings provide critical insights into the scalability and long-term viability of VPSA for carbon capture.

2. MATERIALS AND METHODS

2.1. Materials and Instrumentation

In this study, the MOF MIL-160(Al), processed into shaped granules, was selected for CO_2/N_2 separation under postcombustion conditions. Detailed protocols for its synthesis, shaping procedure, and physicochemical characterization are available in.[30] Textural characterization of the shaped samples was performed by N_2 adsorption at 77 K (Figure S1, Supporting Information), and the Brunauer−Emmett−Teller (BET) specific surface area was determined accordingly (Table 1). These measurements were conducted at the University of Málaga (Spain) using a Micromeritics ASAP 2020 instrument (v4.02). In addition, mercury intrusion porosimetry was carried out with a Micromeritics AutoPore IV 9500 over a pressure range of 0.20−61,000 psia to determine the total intrusion volume, pore area, pore diameter, density, and porosity (Table 1). However, gases utilized for the experiments, including carbon dioxide (99.99%), nitrogen (99.95%), and high-purity helium (99.999%), were sourced from Air Liquide.

Table 1. Characteristics of the Studied Adsorbent (Al-Based MOF MIL-160) Accompanied with the Specifications of the Fixed-Bed Adsorption Set-Up in the Lab-Scale[15]

parameter	numerical values
adsorbent properties[1]	
particle radius	1.35×10^{-3} (m)
bulk density at 0.0037 MPa	1.07 (g/cm^3)
median pore diameter (volume) at 7.7 MPa and 0.1 cm^3/g	0.162 (μm)
median pore diameter (area) at 119.8 MPa and 9.7 m^2/g	0.0104 (μm)
average pore diameter (4 V/A)	0.0454 (μm)
apparent (skeletal) density at 206.5 MPa	1.40 (g/cm^3)
total intrusion volume	0.22 (cm^3/g)
total pore area	19.45 (m^2/g)
micropore volume	0.336 (cm^3/g)
the specifications of the fixed-bed adsorption setup	
bed length	6.8 (cm)
bed diameter	2.1 (cm)
bulk bed density	0.463 (g/cm^3)
mass of sample	10.9 (g)
intraparticle porosity	0.31 (m^3_{void}/m^3_{bead})
interparticle or bed porosity	0.48 (m^3_{void}/m^3_{bed})

A series of dynamic breakthrough and cyclic adsorption tests were carried out using a custom-designed dual-column fixed-bed apparatus. A simple scheme of the experimental setup to accomplish breakthrough and PSA experiments is depicted in Appendix A (Supporting Information). For this investigation, a single column was employed to replicate counter-current adsorption dynamics while minimizing system complexity. Precise control of inlet gas flow rates was achieved using mass flow controllers, and outlet flow rates were monitored with a mass flow meter; both devices were calibrated and supplied by Alicat Scientific. Real-time gas composition at the outlet was tracked using an in-line infrared analyzer to assess the separation performance. Temperature changes within the adsorption bed were recorded using a centrally located thermocouple. System pressure was regulated via a backpressure controller (Bronkhorst). A comprehensive summary of the experimental setup and operational parameters is presented in Table 1, with further technical details reported in.[15]

2.2. Experimental Procedures

This investigation employed a consistent fixed-bed adsorption system for both dynamic breakthrough experiments and pressure swing adsorption (PSA) cycles. Fresh MIL-160(Al) samples were activated via helium purge (327.5 N mL/min) during a controlled thermal ramp (1 K/min) to 423 K, followed by an isothermal hold for 12 h to ensure complete removal of adsorbed moisture and residual volatiles. Initial breakthrough tests were performed under precisely controlled conditions (see Supporting Information, Appendix A) to quantify adsorption kinetics and validate subsequent modeling approaches. Building on these results, we implemented a five-stage PSA cycle operating at 318 K and 4.6 bar, consisting of: (1) counter-current nitrogen pressurization, (2) feedstock introduction, (3) CO_2 rinse for purity enhancement, (4) controlled depressurization to ambient pressure, and (5) counter-current nitrogen purge for adsorbent regeneration. It should be noted that the cyclic adsorption experiments were conducted using a feed gas containing 50% CO_2 and long step times. This experimental configuration was intentionally used to enable unequivocal identification of breakthrough behavior and provide reliable data for dynamic model validation. The use of relatively high CO_2 concentration, long step times, and pure component gases during the steps ensures a clear and well-controlled analysis of the dynamic separation behavior, which is essential for a rigorous validation of the developed model. It is worth noting that during the regeneration steps (blowdown and purge), the pressure is reduced to atmospheric pressure. However, due to constraints associated with the existing experimental setup, operation under vacuum conditions is not feasible. However, the objective of this experimental and simulation analysis was not to reach an optimal performance of PSA process, but only to demonstrate the validation of the dynamic simulation model. Nevertheless, the industrial PSA process was designed and evaluated based on a more representative flue-gas composition of 15% CO_2 and 85% N_2. Complete experimental parameters for all PSA trials are documented in Table 2. In addition, a simple schematic diagram of the designed (V)PSA cycle (Figure S5) and a detailed description of the (V)PSA system, with a clear indication of the valves open and closed in each step of the cycle accompanied by the direction of the flow rate (Figure S6) are illustrated in Appendix A.

3. THEORY AND METHODS

3.1. Mathematical Model

A precise and predictive model is essential for simulating and optimizing PSA systems, particularly one that can accurately represent the adsorption equilibrium and transport behavior. In this work, the extended Langmuir isotherm was selected due to its demonstrated capability in accounting for surface heterogeneity and capturing competitive multicomponent adsorption phenomena.[38] The parameters and calibration methods applied are detailed in the Supporting Information (Appendix E).[38−40]

Table 2. Specifications of the Defined Pressure Swing Adsorption Process for Separating CO_2/N_2 at the Lab-Scale Set-Up

PSA steps	PSA variables					
	the studied compositions		flow rate(mL/min)	step time (s)	temperature (K)	pressure (bar)
	CO_2%	N_2%				
pressurization	-	100	800	65	318	1→4.6
feed	50	50	600	350	318	4.6
rinse	100	0	100−400	160	318	4.6
blowdown	-	-	-	240		4.6→1.0
purge	-	100	0−250	240		1.0

Table 3. Characteristics and Specifications of the Designed VPSA Process for CO2/N2 Separation in the Industrial Scale

the bed-specifications of industrial PSA process	
parameter	numerical values
bed volume	12.37 (m3)
bed diameter	1.5 (m)
bed height	7.0 (m)
bed area	1.77 (m2)
bed porosity	0.487 (−)
particle radius	1.35×10^{-3} (m)
bulk bed density	463 (kg·m−3)

PSA steps	PSA variables					
	the studied compositions		flow rate(L/min)	step time (s)	temperature (K)	pressure (bar)
	CO2%	N2%				
pressurization	-	100[a]	35×10^3	150	318	0.2→4.5
feed	15	85	10×10^4	320	318	4.5
rinse	100[a]	0	30×10^3-39×10^3	280	318	4.5
blowdown	-	-	0	80		4.5→0.2
purge	-	100	0.5×10^3-7.5×10^3	250		1.0→0.2

[a] The Pressurization and Purge compositions were according to the Feed out composition, the Rinse composition was according to the blowdown and purge out composition. So, it is not a fixed number, nor 100% of N_2.

To describe the transient behavior of the PSA column, a nonisothermal dynamic model was developed based on conservation principles for mass, energy, and momentum. Several simplifying assumptions were introduced to facilitate numerical computation without compromising essential physics: (i) ideal gas behavior is assumed for the gas phase, (ii) mass transfer is modeled using a lumped resistance approach, (iii) heat transfer occurs adiabatically, neglecting conduction within the solid phase, (iv) pressure drop is calculated via the Ergun equation, and (v) axial dispersion is incorporated using the Langer formulation.[40,41] A comprehensive description of the model equations and relevant assumptions is provided in the Supporting Information. Also, the characteristics and specifications of the designed VPSA process for CO_2/N_2 separation on the industrial scale are reported in Table 3.

The PSA simulations were conducted under experimentally relevant boundary conditions, as outlined in Table S3 (Supporting Information). Four major performance metrics—purity, recovery, productivity, and energy consumption—were used to evaluate the system, following the definitions in eqs 1−5. These indicators offer a quantitative basis for comparing different operating scenarios.[21]

$$N_2\text{purity}(\%) = \frac{\sum_j \left(\int_0^{t_j} F_{N_2,\text{out}} dt \right)}{\sum_j \left(\int_0^{t_j} F_{N_2,\text{out}} dt + \int_0^{t_j} F_{CO_2,\text{out}} dt \right)} \times 100 \tag{1}$$

$$N_2\text{rec}(\%) = \frac{\sum_j \left(\int_0^{t_j} F_{N_2,\text{out}} dt \right) - \sum_k \left(\int_0^{t_k} F_{N_2,\text{in}} dt \right)}{\sum_l \left(\int_0^{t_j} F_{N_2,\text{in}} dt \right)} \times 100 \tag{2}$$

$$CO_2\text{purity}(\%) = \frac{\sum_m \left(\int_0^{t_m} F_{CO_2,\text{out}} dt \right)}{\sum_m \left(\int_0^{t_m} F_{CH_4,\text{out}} dt + \int_0^{t_m} F_{CO_2,\text{out}} dt \right)} \times 100 \tag{3}$$

$$CO_2\text{rec}(\%) = \frac{\sum_m \left(\int_0^{t_m} F_{CO_2,\text{out}} dt \right) - \sum_m \left(\int_0^{t} F_{CO_2,\text{in}} dt \right)}{\sum_l \left(\int_0^{t_l} F_{CO_2,\text{in}} dt \right)} \times 100 \tag{4}$$

$$\text{Productivity}(\text{molkg}^{-1}\text{h}^{-1}) = \frac{\sum_j \left(\int_0^{t_j} F_{CO_2,\text{out}} dt \right) - \sum_k \left(\int_0^{t_k} F_{CO_2,\text{in}} dt \right)}{\text{mass of dry adsorbent} \times t_{\text{cycle}}} \tag{5}$$

Here, l is the Feed, counter-current Pressurization, j is the Feed, Rinse, k is the Purge, countercurrent Pressurization, and m is the Blowdown and Purge.[20,21] Energy consumption for each configuration was computed using eq 6, which considers parameters such as molar flow rates, thermodynamic properties of the gas, pressure differentials, and the efficiencies of vacuum pump (η = 60%) and compressor and (η = 80%).[42]

$$\text{Energy consumption} = \frac{1}{\eta} \dot{n} R_g T_g \frac{\gamma}{\gamma - 1} \left(\left(\frac{P_H}{P_L} \right)^{\gamma - 1/\gamma} - 1 \right) \tag{6}$$

Here, ṅ is the molar flow rate, R_g is the ideal gas constant, T_g the gas temperature, η is the pump or compressor efficiency, γ is the specific heat ratio of the gas $\left(\gamma = \frac{C_P}{C_V} \right)$, as well P_L and P_H indicate the lower and higher pressures, respectively.[21,42] However, more details regarding the considered parameters to estimate the energy consumption through compression and vacuum are discussed in Table S1 (Appendix A). It is worth noting that the numerical integration of the system equations was performed in the gPROMS environment using a second-order orthogonal collocation scheme, with 28 finite elements applied for spatial discretization to ensure computational accuracy and convergence.

Finally, to manage the competing performance criteria of the process, a discrete-data-driven optimization framework was implemented, targeting simultaneous enhancement of the CO_2 purity, recovery, and energy demand. Prior to optimization, all target variables were normalized to eliminate scale bias and ensure proportional influence. A weighted summation model was then formulated to consolidate these metrics into a unified performance indicator, effectively converting the multiobjective scenario into a single-objective optimization task. The weighting factors were defined according to process-specific goals, enabling flexible prioritization. By systematically scanning the discrete solution space, the algorithm identified configurations that provided an optimal compromise among the three objectives. This approach proved to be particularly effective for resolving trade-offs in complex adsorption systems, where improving one metric often adversely affects the others. It is noteworthy that because purge/rinse directly control regeneration and internal reflux, excessively high values increase recycled gas volumes and vacuum/compression duty, whereas insufficient values reduce working capacity and productivity. Optimizing these steps therefore supports lower long-term OpEx by reducing specific energy while maintaining target separation performance.

3.2. Techno-Economic Assessment (TEA)

In this work, CapEx estimation begins with determining the free-on-board (FOB) costs of equipment based on design specifications and evaluations performed using the ASPEN Economic Analyzer. All major process equipment is considered, and the collective FOB cost constitutes the basis for further calculations. To account for freight costs, 10% is added to the total FOB, resulting in the delivered purchased cost (DPC).[36] Table S1 (Supporting Information) summarizes the FOB and DPC values for the principal equipment. To update the DPC to current-year values, the Chemical Engineering Plant Cost Index (CEPCI) factors are applied using the following relation, in which CEPCI_1 and CEPCI_2 represent the CEPCI factor in years 1 and 2, respectively. Also, CapEx_1 is the capital cost in year 1 and CapEx_2 indicates the capital cost in year 2.

$$\frac{\text{CEPCI}_1}{\text{CEPCI}_2} = \frac{\text{CapEx}_1}{\text{CapEx}_2} \tag{7}$$

From eq 7 and CEPCI_1 and CEPCI_2 are equal to 797.9 and 800.2, respectively; the updated DPC resulted in \$2199.50 thousand in 2024.

From the total DPC, direct and indirect costs, as well as interest during construction, are calculated using standard multipliers, as presented in Table 4.

Table 4. Estimated Direct and Indirect Costs in the Developed Topology in 2024

activities	multiplier	cost (\$)
direct cost calculation		
delivered purchased cost (DPC)	-	2.2×10^6
installation	0.43 DPC[a]	9.45×10^5
piping	0.66 DPC	1.45×10^6
instrumentation & control	0.4 DPC	8.79×10^5
insulation	0.03 DPC	6.6×10^4
electrical systems	0.1 DPC	2.2×10^5
buildings	0.47 DPC	1.03×10^6
yard improvement	0.2 DPC	4.4×10^5
utilities	0.5 DPC	1.09×10^6
off-site	0.2 DPC	4.4×10^5
landIndirect cost calculation	0.08 DPC	1.75×10^5
indirect cost calculation		
design & engineering	0.25 DC[b]	2.24×10^6
construction	0.35 DC	3.13×10^6
contractor's fee	0.08 DC	7.16×10^5
contingency	0.40 DC	3.58×10^6
start-up	0.03 DC	2.69×10^5

[a] DPC: Delivered purchased cost. [b] DC: Direct Cost.

The interest during construction is determined using eq 8, applying a standard annual interest rate of 5%.[43] This results in an estimated interest cost of \$222,149.70.

$$\text{Interest} = \text{Intesrestrate} \times 2.02 \times \text{DPC} \tag{8}$$

Based on the aggregated data, the total CapEx is calculated as \$18.89 × 10^6. The annualized capital cost is then computed using eq 9

$$\text{AnnualizedCost} = \text{Cap } Ex \times \frac{j(1+j)^n}{(1+j)^n - 1} \tag{9}$$

Here, n denotes the plant lifetime and j represents the interest rate. However, due to the process simplicity, we can consider 30 years as the plant lifetime,[44] but the plant lifetime and the interest rate are considered 15 years and 5%, respectively,[43] which leads to an annualized CapEx of \$ 1,819.99 thousand.

In the next step, OpEx is estimated, which includes both variable operating costs (VOC) and fixed operating costs (FOC). VOC encompasses the cost of continuously consumed utilities such as electricity (\$0.12/kWh) and adsorbents (\$55/kg), the latter of which requires replacement every 1.5 years due to degradation during pressure swing adsorption cycles.[43,44]

On the other hand, FOC comprises labor, maintenance, taxes and insurance, overheads, and working capital. Labor costs are calculated based on an hourly rate of \$34.50 per operator. A detailed breakdown of the VOC and FOC components is provided in Table 5. Also, the detailed specifications of employed assumptions and considered constants in calculating OpEx are reported in Table 6. Finally, the Final Annualized Cost (FAC) is derived from the sum of annualized CapEx and OpEx, thereby offering a comprehensive financial outlook for the proposed CO_2 capture process.

Table 5. Detailed Description of Key Calculated Fixed and Variable Operating Costs

parameter		multiplier	cost (k\$/y)
variable operating cost (VOC)	electricity	-	related to conditions
	total adsorbent cost	-	242
fixed operating cost (FOC)	labor	-	554
	maintenance	0.07 DPC	151
	taxes & insurance	0.03 DC	75
	overhead	0.017 DC	38
	financial working capital	0.09 * 1/12 variable operating cost	related to VOC

Table 6. Detailed Specifications of Employed Assumptions and Considered Constants in Calculating OpEx

parameter	quantity
electricity price in Portugal at 2024	0.12 \$/kWh
labor	34.5 \$/person.h[45]
number of operators	2 people[46]
working shift	4[46]
annual working days	335
MOF unit price	55 \$/kg[32]
MOF replacement period	1.5 y
bed porosity	0.487
bed bulk density	463 kg/m^3

4. RESULTS AND DISCUSSION

4.1. Lab Scale Adsorption Experiments

Breakthrough and cyclic PSA experiments were conducted to probe the separation performance of shaped MIL-160(Al) for CO_2/N_2 mixtures under flue-gas conditions (See Appendix A). Also, the column and adsorbent characteristics are summarized in Table 1. The accomplished breakthrough experiments and sample characteristics ensured reproducibility across the 24 lab-scale PSA experiment runs (all accomplished PSA experiments accompanied by all details and specifications are illustrated in Appendixes C&D), while the intrinsic selectivity of MIL-160(Al) toward CO_2 provided the basis for efficient separation.[15]

4.1.1. Single-Variable Effects. The influence of purge and rinse on separation is illustrated in Figure 1. As shown in Figure 1a, increasing the purge flow rate from 25 to 250 mL/min consistently decreased CO_2 purity from 91% to 49%. In fact, a higher purge flow primarily enhances the desorption of the strongly adsorbed CO_2, while potentially entraining weakly

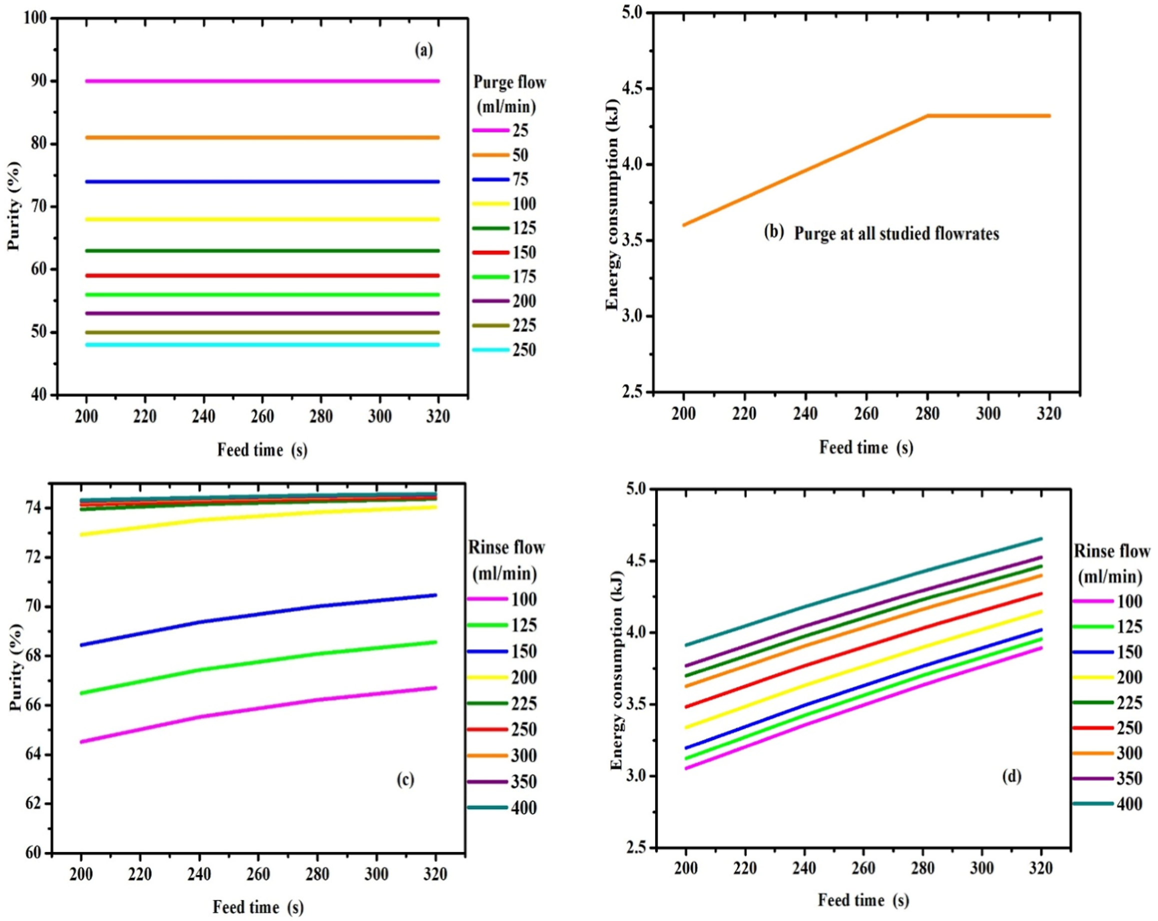

Figure 1. Impact of different purge flow rate (rinse flow rate: 300 mL/min) in the lab-scale on (a) the purity of CO_2 and (b) the energy consumption, as well as the impact of different rinse flow rates (at purge flow rate: 75 mL/min) in the lab-scale on (c) the purity of CO_2 and (d) the energy consumption (for steady state cycle: No:7).

adsorbed N_2 into the CO_2 product stream, thereby diluting its purity. On the other hand, as can be observed in Figure 1b, at low purge flow rates, energy demand rises steeply because the pump must overcome significant resistance to achieve regeneration. As time is increased, regeneration becomes more effective, and the energy per unit of CO_2 captured stabilizes, leading to a plateau. Beyond this point, additional purge does not significantly increase the desorbed volume or improve regeneration efficiency, so energy consumption flattens. This behavior reflects the diminishing returns of vacuum work once the adsorbent approaches full regeneration. The plateau thus defines a practical upper limit for purge, where further intensification provides no energetic advantage.

In contrast, rinse flow rate had the opposite effect: purity improved significantly with increasing rinse flow rate from 100 to 400 mL/min (Figure 1c). The rinse stream displaced N_2 from the outlet voids and sharpened the adsorption front, reducing nitrogen slip into the CO_2-rich product. However, energy consumption (Figure 1d) rose sharply at higher rinse flows because of the additional compression duty required. Thus, while the rinse is favorable for product quality, its optimization must consider energy trade-offs. These findings establish a fundamental mechanistic contrast: purge penalizes CO_2 purity but restores capacity, whereas rinse enhances CO_2 purity but raises energy demand.

4.1.2. Two-Variable Interactions.

The coupled effects of purge and rinse are depicted in Figure 2, which presents contour maps of purity, recovery, productivity, and energy consumption. The purity map (Figure 2a) shows that increasing the level of rinse at moderate purge yields the highest CO_2 purity. However, recovery trends (Figure 2b) confirm that higher purge flows cause substantial recovery penalties, while a higher rinse slightly offsets losses by limiting N_2 contamination but cannot compensate for the inherent CO_2 displacement during regeneration. Also, productivity (Figure 2c), as one could expect, represents a strong dependency on purge flow, while it is almost constant at different rinse flow rates. Energy consumption (Figure 2d) rose steeply at high rinse (compressor-intensive) and at high purge (vacuum-intensive), reinforcing that both extremes are economically unfavorable.

4.1.3. Model Validation at CSS.

Simulated and experimental cyclic steady-state (CSS) profiles are compared in Figure 3. The model successfully captured pressure swings, adsorption- and desorption-induced temperature excursions, and outlet flow variations. The correct representation of adsorption heats in the thermal profiles and accurate depiction of flow dynamics demonstrate the reliability of the model to predict real system performance. This validation is essential, as it underpins the credibility of scale-up to industrial conditions and the subsequent techno-economic analysis.

4.2. Industrial VPSA for CO_2/N_2 Separation

The transition from laboratory PSA cycles to an industrial VPSA unit requires careful adaptation of the operating conditions and

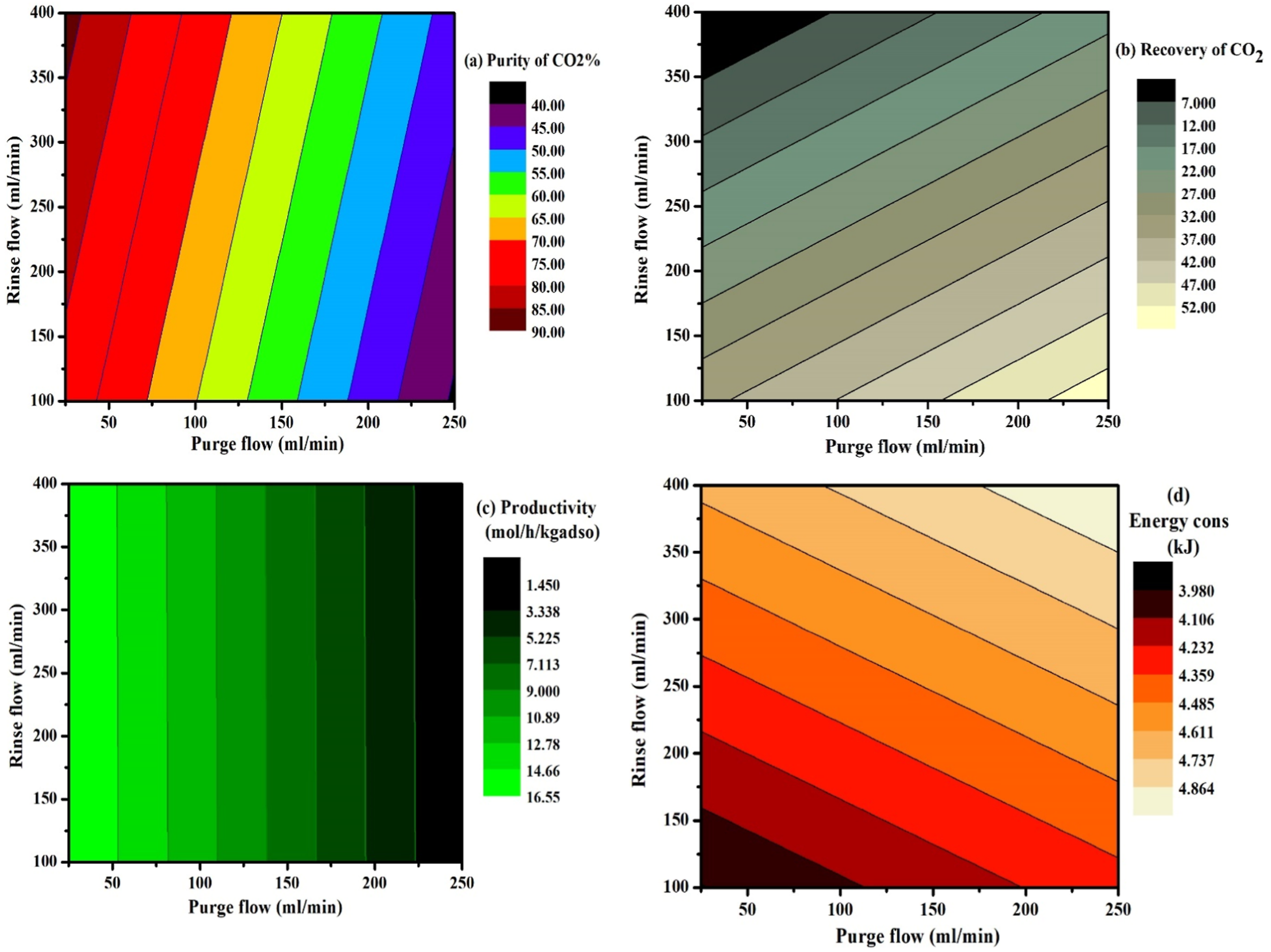

Figure 2. Counter graphs of (a) the purity, (b) the recovery, (c) the productivity and, (d) the energy consumption of CO_2 as a function of rinse and purge flow rates in the accomplished PSA experiments in the lab-scale (at the feeding time: 320s).

equipment constraints. The VPSA design employed here (Table 3) was deliberately chosen to reflect practical industrial layouts, where overlapping pressurization and regeneration steps enable near-continuous operation. Unlike lab-scale beds, industrial units must contend with pressure-drop scaling, axial and radial maldistribution, and the nonideal efficiency of vacuum and compression machinery. These factors impose nontrivial penalties on both purity and energy use, meaning that direct extrapolation from lab results can be misleading unless supported by validated dynamic modeling (Figure 3). For MIL-160(Al), whose structured shaping provided robust mechanical stability,[15,30] the challenge lies less in attrition resistance and more in balancing purge and rinse intensities to minimize power consumption without compromising separation performance.

4.2.1. D.B.A. Effect of Purge Flow Rate on Separation Performance.

The influence of purge flow rate on separation performance is shown in Figure 4a,b. As purge flow increased from 500 to 7.5×10^3 L/min, CO_2 purity decreased from 91% to 82%, due to overdesorption of CO_2 molecules together with N_2 during regeneration. This stripping effect becomes more pronounced at larger purge rates because the deeper vacuum and stronger purge stream mobilize CO_2 from the adsorbent micropores. Energy consumption (Figure 4b) exhibited a monotonic increase with purge flow rate. This trend reflects the higher duty required from the vacuum system, which must process larger volumes of gas at reduced pressures. At the industrial scale, vacuum pump efficiency deteriorates sharply at high throughputs, compounding the energy penalty. Thus, high purge flow rates are scientifically undesirable for two reasons: they both reduce CO_2 purity/recovery and impose escalating energy costs. The alignment between purity and energy penalties emphasizes that purge minimization is central to industrial viability.

4.2.2. D.B.B. Role of Rinse Flow Rate in Process Optimization.

The role of rinse flow is illustrated in Figure 4c,d. Unlike the purge, the CO_2-rich rinse stream sweeps CO_2 through the bed to displace N_2, preventing it from slipping into the product. This polishing effect is particularly valuable for flue gas mixtures where the CO_2 partial pressure is low and adsorption fronts are relatively shallow. However, energy consumption increased significantly with rinse flow rate (Figure 4d). The sharp rise is explained by the compressor duty required to deliver large rinse flows at an elevated pressure. Unlike vacuum pumps, compressors at the industrial scale maintain reasonably high isentropic efficiencies, but the quadratic relationship between flow rate and energy input still results in a steep energy penalty. Importantly, the rate of purity improvement diminishes at higher rinse flows, whereas energy

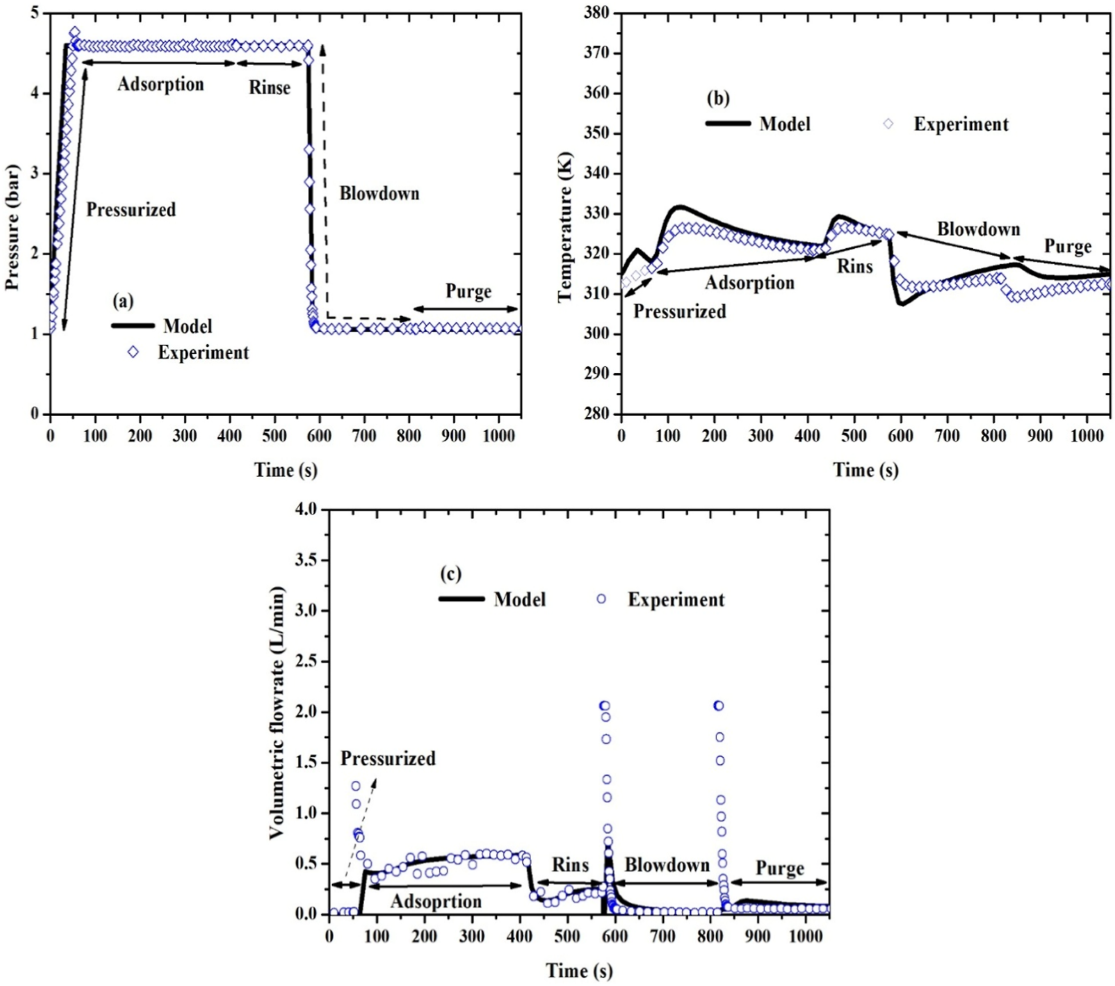

Figure 3. Experimental and modeling results: (a) pressure, (b) temperature history, and (c) total volumetric flow rate of the best accomplished PSA experiment in the lab-scale.

consumption continues to increase nearly linearly, producing an unfavorable trade-off beyond a certain threshold.

It is worth noting that compared with traditional adsorbents such as zeolite 13X or activated carbon (see Table S4, Appendix F), MIL-160(Al) demonstrates competitive separation with lower heats of adsorption,[15] thereby reducing temperature excursions during cycling. This advantage mitigates thermal management challenges that often amplify energy requirements on a large scale. However, the trends observed in Figure 4b,d make clear that the system remains highly sensitive to utility loads, suggesting that MIL-160(Al) must be paired with carefully optimized rinse/purge strategies to leverage its material benefits fully. The strong dependence of energy consumption on purge (Figure 4b) and rinse (Figure 4d) directly explains why the techno-economic analysis in Section 4.3 identifies electricity price as the single most influential variable. The scale-up results establish that minimizing purge while operating at moderate rinse is not only technically optimal but also economically decisive, as both choices, on one hand, directly constrain compressor and vacuum energy consumption, the dominant contributors to operating expenditure; but on the other hand, lower purge flow leads to a smaller compressor with lower DPC.

The two-dimensional contour maps in Figure 5 present the combined impact of rinse and purge flow rates on the four critical key performance indicators (KPIs): CO_2 purity (5a), recovery (5b), productivity (5c), and energy consumption (5d). Taken together, these maps reveal not only the operational trade-offs but also the physical mechanisms that govern the VPSA process on a scale. As shown in Figure 5a, the CO_2 purity increases with a rinse and decreases with a purge. Mechanistically, an increased rinse displaces residual N_2 from the column voids and from the near-product portion of the MTZ, sharpening the CO_2 front and reducing the light-component slip at the product outlet. This "polishing" effect is the strongest at low-to-moderate rinse (large marginal gains at first) and exhibits diminishing returns as the MTZ becomes fully sharpened. Conversely, applying a purge (vacuum/regenerative flow from the light end) removes adsorbed components to regenerate capacity but also entrains CO_2 from the adsorbed phase. As purge intensity grows, the fraction of adsorbed CO_2 removed into the purge stream increases, which dilutes the subsequently collected product and therefore lowers the measured product purity. These countervailing mechanisms explain the ridge of high-purity values in the high-rinse/low-purge portion of the map.

On the other hand, as represented in Figure 5b, the recovery landscape demonstrates a strong dependence on both purge and rinse flow rates. At a low purge, recovery remains limited because incomplete regeneration leaves a significant fraction of adsorption sites occupied by N_2 and residual CO_2, thereby reducing the effective working capacity for subsequent feed steps. As the purge flow rate increases, recovery improves

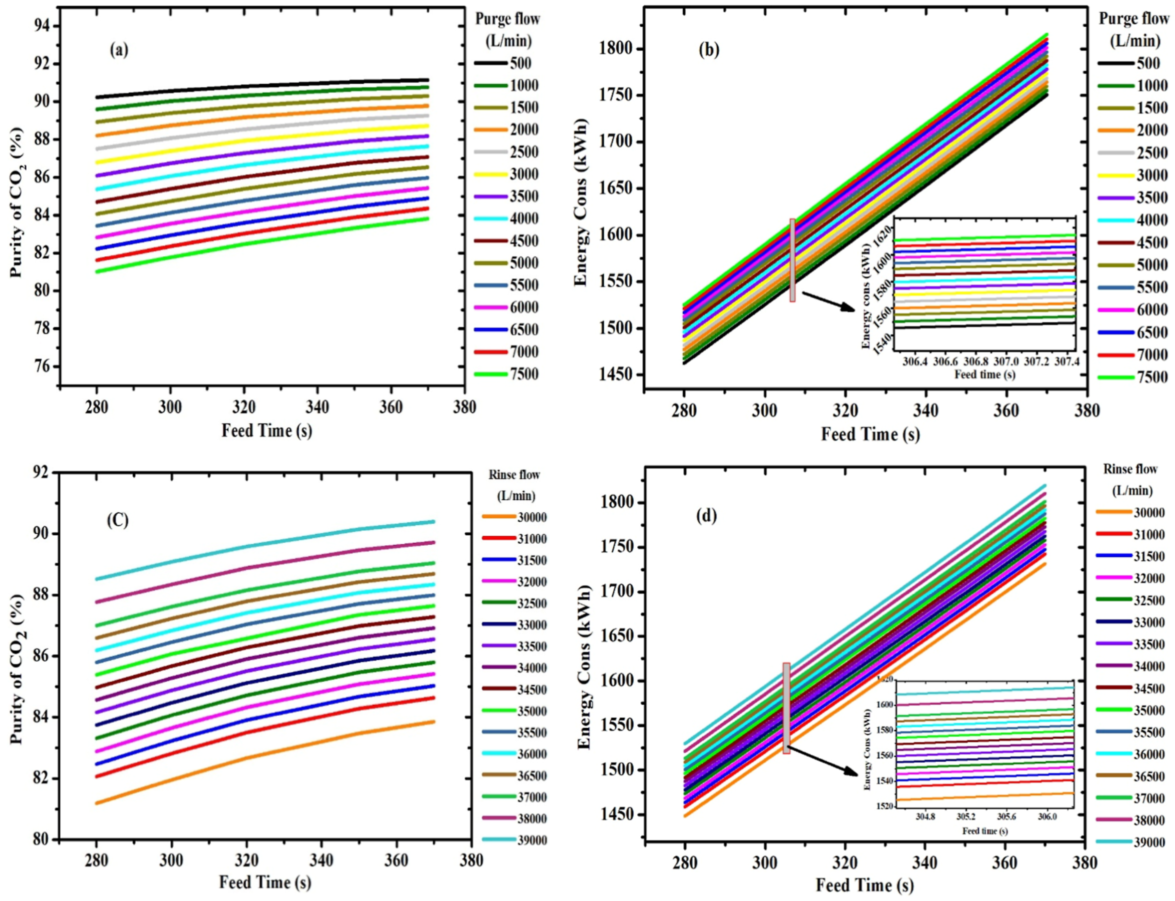

Figure 4. Impact of different purge flow rates (at rinse flow: 35000 L/min) in the industrial scale on (a) the purity of captured CO_2 from flue gas, and (b) the energy consumption, as well as the impact of different rinse flow rates (at purge flow: 4000 L/min) in the industrial scale on (c) the purity of captured CO_2 from flue gas, and (d) the energy consumption (for steady state cycle: No:28).

because regeneration becomes more effective: additional CO_2 can be adsorbed during the next feed period, enhancing the overall amount of CO_2 captured. However, this benefit is counteracted by the influence of rinsing. Higher rinse flows, while beneficial for product purity (see Figure 5a), tend to reduce recovery because a portion of CO_2 is displaced into the rinse stream or diverted from the product outlet. Consequently, recovery reaches its maximum under conditions of moderate purge and minimal rinse, illustrating the inherent tension between purity enhancement and recovery maximization. This trend is consistent with the fundamental thermodynamics of PSA cycles, where regeneration strength governs the available adsorption capacity while auxiliary steps such as rinsing redistributed product gas at the expense of net yield.

As already discussed, productivity, defined as the moles of CO_2 recovered per unit adsorbent volume and per unit cycle time, is predominantly controlled by purge intensity and is relatively insensitive to rinse flow within the studied range, as illustrated in Figure 5c. Increasing purge reduces productivity because, although recovery initially improves, excessive purge flow simultaneously removes a significant fraction of adsorbed CO_2 into the waste stream and extends the duration or intensity of regeneration steps. Both mechanisms lower the net CO_2 throughput per unit of time. In contrast, rinse has little effect on productivity, since its primary function is to improve product quality rather than influence the gross mass of CO_2 adsorbed and desorbed. Thus, productivity remains nearly constant across the tested rinse levels, highlighting that productivity penalties are primarily associated with purge operation. This observation underscores the importance of minimizing unnecessary purge intensity in industrial systems, as productivity losses translate directly into larger column inventories and higher capital costs for achieving a target capture rate.

Regarding energy consumption, as demonstrated in Figure 5d, energy consumption rises with both purge and rinse flows, though for different mechanistic reasons. Increased purge flow imposes a heavier burden on the vacuum system, which must evacuate larger volumes of gas at subatmospheric pressures. Since the specific work of vacuum pumping scales with the logarithm of the pressure ratio and efficiencies decline under high-throughput, deep-vacuum conditions, the energy cost of purge rises sharply with intensity. Conversely, rinse flow increases compressor duty as larger volumes of gas must be recompressed and delivered at an elevated pressure to the bed. At the industrial scale, where flow rates are extremely large, even moderate increments in rinse translate into substantial increases in compression work, amplified by quadratic dependence of pressure-drop losses on velocity. The combined effect is a nonlinear escalation of energy demand as either variable is intensified, with the highest penalties occurring in the high-purge/high-rinse corner of the operating space. These findings confirm that utility consumption is the dominant operational barrier in rinse-assisted VPSA and reinforce the necessity of identifying an interior operating window where CO_2 purity and recovery are acceptable, but energy demand is minimized.

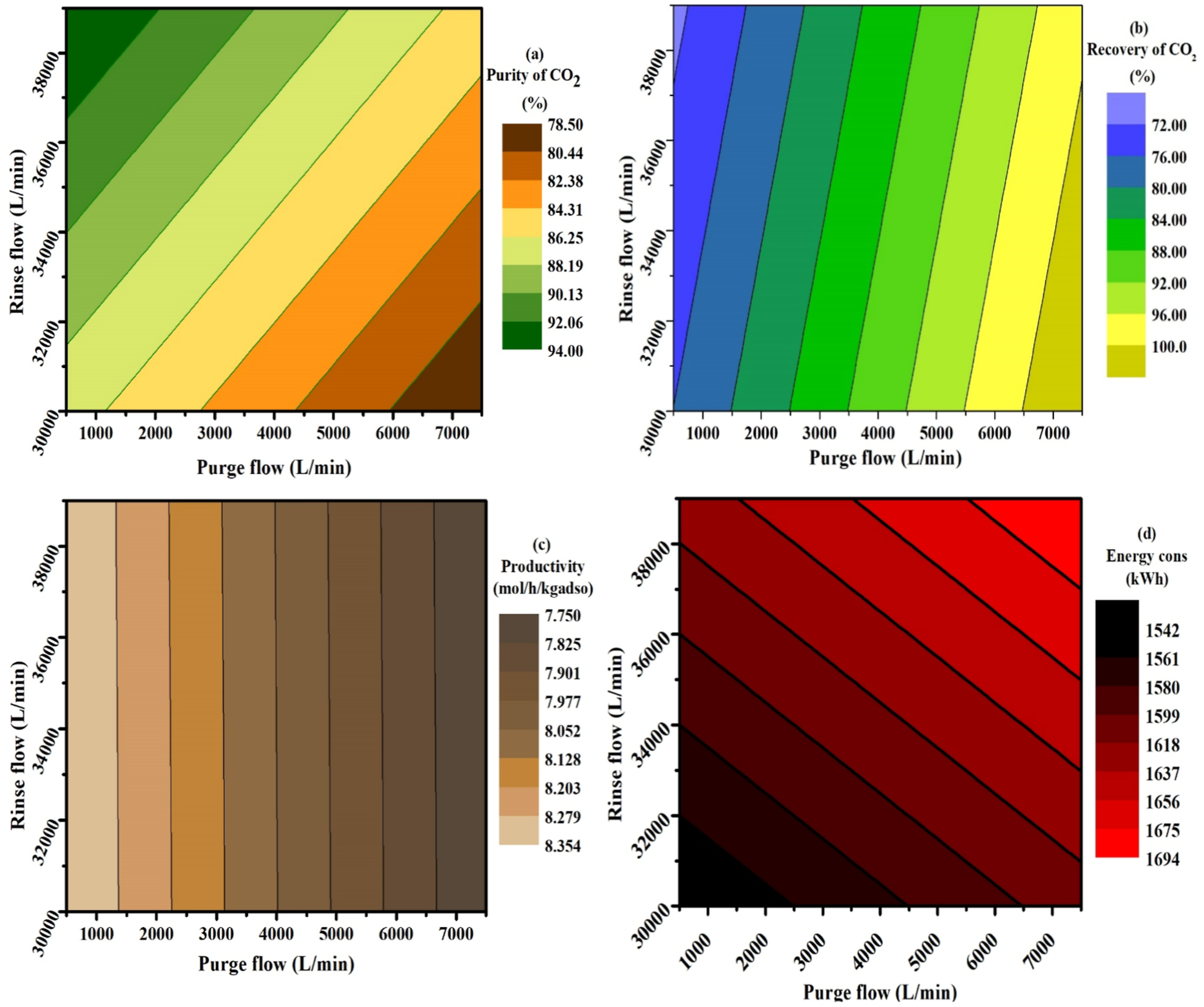

Figure 5. Counter graphs of (a) the purity, (b) the recovery, (c) the productivity and, (d) the energy consumption of carbon dioxide as a function of rinse and purge flow rates (at the feeding time: 320s).

4.3. Techno-Economic Assessment (TEA)

In this study, the economic model follows a bottom-up costing workflow. Equipment FOB costs (ASPEN-derived) were increased by 10% freight to obtain the Delivered Purchased Cost (DPC), then DPC was updated to 2024 price levels using CEPCI factors, and standard direct and indirect multipliers were applied to obtain the total CapEx (Table 4 and eq 7). Annualization of CapEx uses the capital recovery factor (eq 9) with a base case lifetime and discount rate of 15 years and 5%, respectively. Operating expenses were partitioned into variable operating costs (VOC: electricity and adsorbent replacement) and fixed operating costs (FOC: labor, maintenance, taxes and insurance, overhead and working capital). The Final Annualized Cost (FAC) is defined as the sum of annualized CapEx and OpEx. Key parameter values used in the baseline case include an electricity price of 0.12 \$/kWh, MOF unit price of 55 \$/kg and MOF replacement every 1.5 years.

4.3.1. D.C.A. Capital Expenditure (CapEx) Analysis. The bottom-up capital estimate yields a DPC of ≈\$2.20 M (delivered purchased cost), and after applying installation, piping, instrumentation, buildings, utilities, and standard indirect multipliers, the total plant CapEx is calculated as \$18.89 M. Annualizing this CapEx with the chosen lifetime/discounting produces an annualized capital charge of ≈\$1.82 M·yr^{-1}. These results and the decomposition by the multiplier are reported in Table 4. Two practical implications follow from the CapEx breakdown. First, the process is equipment-intensive: compressors, vacuum pumps and balance-of-plant occupy a very large share of the DPC and therefore the CapEx. Second, standard multipliers (installation, piping, instrumentation etc.) amplify the FOB/DPC base; i.e., modest reductions in primary equipment cost (e.g., more compact compressors, lower pressure-ratio machines, or smaller beds) propagate nonlinearly into the total CapEx. These behaviors underscore why process choices that reduce required flow rates and pressure ratios (and hence compressor sizing) deliver outsized capital savings.

4.3.2. D.C.B. Operating Expenditure (OpEx) Breakdown. Table 5 summarizes the OpEx components calculated for the baseline configuration. Using the values in Table 5, the fixed operating costs, except working capital (e.g., labor + maintenance + taxes and insurance + overhead), sum to ≈ \$819.6 k·yr^{-1}, while the calculated annual adsorbent replacement cost is \$242.7 k·yr^{-1} (baseline 1.5-yr replacement with MIL-160 at \$55·kg^{-1}), giving a nonenergy OpEx total of ≈ \$1,062.3 k·yr^{-1}. Adding the annualized CapEx (≈\$1,819.99 k·yr^{-1}) produces a baseline FAC excluding electricity of ≈\$2.88 M·yr^{-1} (i.e., \$1.82 + \$1.06 M). Accordingly, we can have

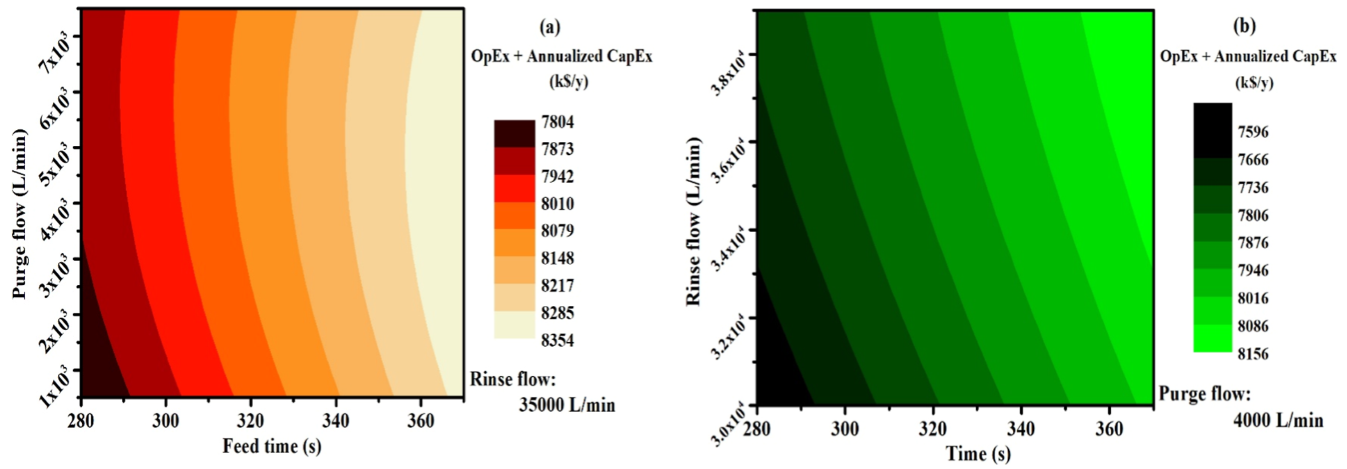

Figure 6. Evaluation of (a) the effect of purging flow rate on the FAC at varying feed durations and (b) the effect of rinsing flow rate on the FAC across different feed times.

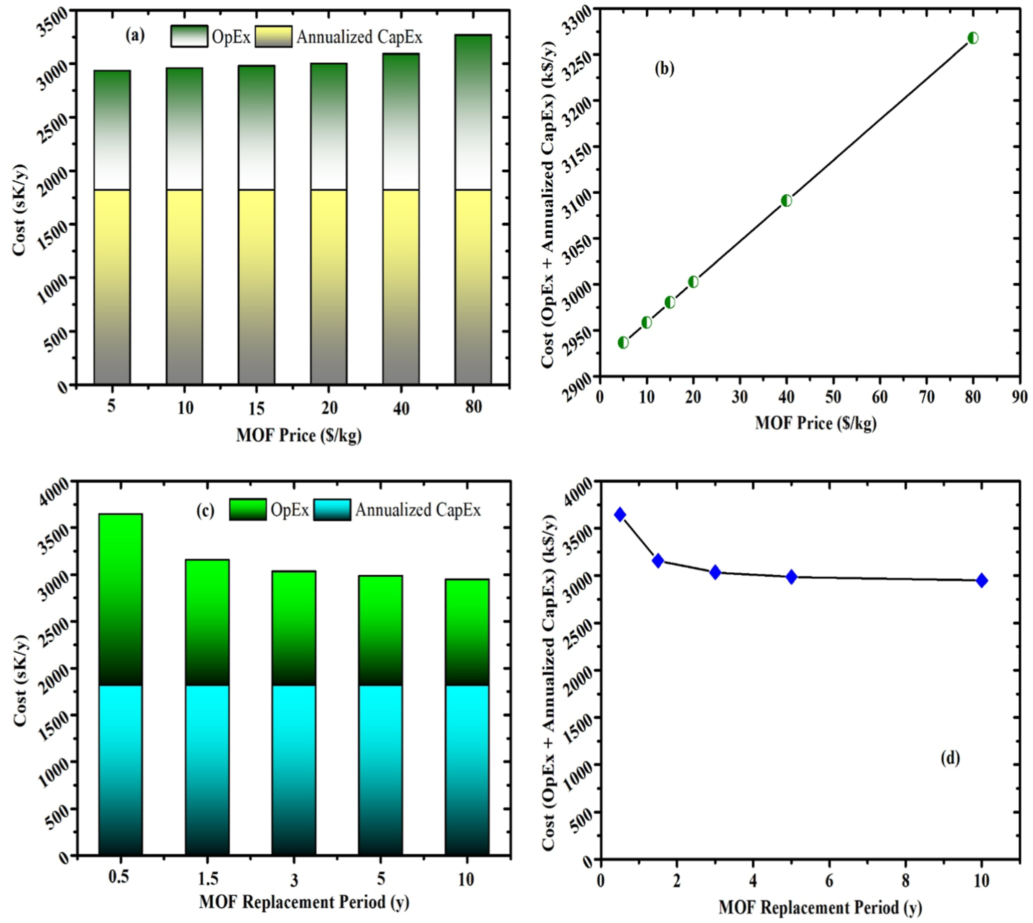

Figure 7. Influence of MOF price on (a) operating expenses (OpEx) and annualized capital expenditures (CapEx) and (b) the FAC. The impact of MOF replacement interval on (c) OpEx and annualized CapEx, and (d) Cost (OpEx + Annualized CapEx).

- Fixed operating cost (FOC) except working capital ≈\$819.6 k·yr^{-1} (labor 554.8; maintenance 151.3; taxes and insurance 75.7; overhead 37.8).
- Adsorbent replacement (baseline) ≈\$242.7 k·yr^{-1}.
- Annualized CapEx ≈\$1,819.99 k·yr^{-1}.

4.3.3. D.C.C. Sensitivity Analysis and Dominant Cost Drivers. The FAC dependence on purge and rinse flow rates is demonstrated in Figure 6. The FAC contour maps show an interior minimum (i.e., a Pareto-type optimum) as a function of the purge and rinse rates. Economically meaningful minima exist because purge and rinse have opposing effects on product quality, recovery, and energy use. In the baseline scans, the FAC minimum appears at moderate purge and high-to-moderate rinse (maps in the article), reflecting the compromise between: (i) product quality gains from effective rinsing (which reduces the required number of beds and mitigates downstream

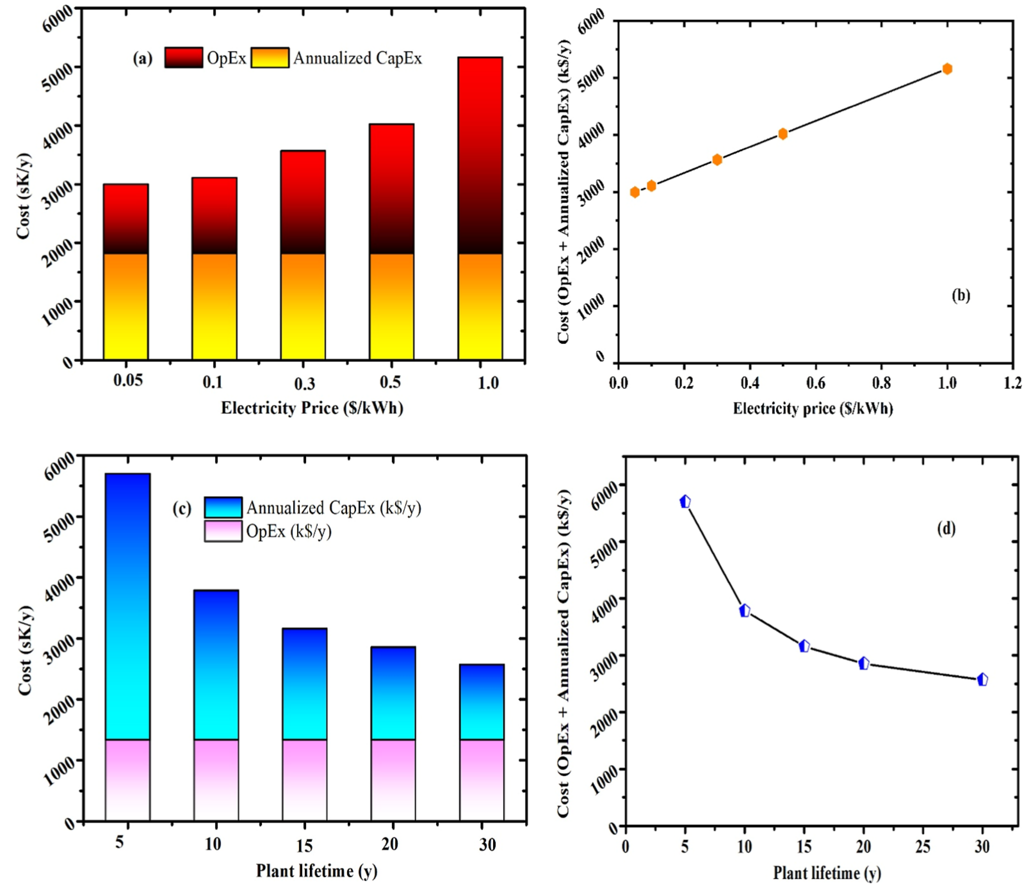

Figure 8. Effect of electricity price on (a) operating expenses (OpEx) and annualized capital expenditures (CapEx), and (b) the FAC. Also, the influence of plant lifetime on (c) OpEx and annualized CapEx, and (d) the FAC.

polishing duty) and (ii) the energy penalty from larger purge and rinse volumetric flows that directly increase compressor and vacuum work via the adiabatic compression relation and through pressure-drop growth (Ergun dependence). Thus, the FAC minimum is not at the lowest possible energy point nor at the highest purity point but at the operating point that minimizes the sum of annualized CapEx and OpEx.

In this way, Figure 7 represents the influence of the MOF price and MOF replacement interval on OpEx and CapEx. It is noteworthy that the sensitivity range for MOF price was selected by considering the cost of MIL-160(Al) (55 $/kg) and benchmarking against reported cost estimates for other MOFs in the literature.[47] As can be observed in Figure 7a, the OpEx increases essentially linearly with the MOF unit price because the adsorbent replacement is accounted for as a variable operating cost in the TEA (Table 5), not as a capitalized inventory. Thus, changing the $/kg enters OpEx through the replacement line item without affecting equipment-related capital charges. Consistent with the accounting adopted in Section "Operating Expenditure (OpEx) Breakdown", the annualized CapEx curve is flat across the explored price range because equipment costs are independent of adsorbent price by construction (Tables 5, 6). The baseline flue-gas case already shows a sizable adsorbent line (total adsorbent cost = 242.70 k $/y), so even moderate price swings can measurably shift OpEx, while leaving CapEx unchanged (Figure 7a; Table 5). It is worth noting, as demonstrated in Figure 7b, because FAC = annualized CapEx + OpEx, the slope of FAC vs $/kg mirrors the OpEx sensitivity, while the intercept is set by the (unchanged) annualized CapEx. Consequently, the adsorption material price acts as a first-order lever on FAC only to the extent that the adsorbent share within OpEx is non-negligible under the chosen operating point. Regarding the impact of sorbent replacement interval, as shown in Figure 7c, extending the replacement interval reduces the frequency-weighted adsorbent spend per year, thereby lowering OpEx almost inversely with interval length, while the annualized CapEx remains constant (again reflecting the separation between equipment capital and consumables). This effect is particularly relevant for MOFs, for which stability improvements (e.g., moisture/thermal robustness) translate directly into fewer replacements per lifetime and, therefore, into lower OpEx. Indeed, as represented in Figure 7d, as the MOF replacement interval increases, the total cost (OpEx + annualized CapEx) decreases due to a lower annualized adsorbent expenditure, while the capital charge remains constant. The decline is nonlinear, with diminishing benefits at longer intervals since CapEx dominates the cost structure. This indicates that extending the adsorbent lifetime provides consistent, though incremental, economic gains. The result highlights the importance of MOF stability improvements as a complementary lever to energy reduction strategies. It is noteworthy that comparing other technologies for CO_2 capture from flue gas or other sorbents,[48,49] MIL-160(Al) demonstrates an appealing capacity for commercial scale applications.

Figure 8 illustrates the dual external sensitivities of the VPSA process—electricity tariff and plant lifetime—on both cost structure and total economics. As shown in Figure 8a, OpEx increases linearly with electricity price, reflecting the direct proportionality between energy cost and compressor/vacuum pump duty, whereas annualized CapEx remains constant because equipment costs are unaffected by tariffs. This relationship propagates into Figure 8b, where the FAC also rises linearly with the electricity price, confirming that power tariffs are the dominant external risk factor for capturing economics. In contrast, Figure 8c shows that extending the plant lifetime has no influence on OpEx but significantly reduces the annualized CapEx, with diminishing returns at longer horizons as the CapEx contribution becomes diluted relative to annual operating expenses. Consequently, Figure 8d reveals that the FAC decreases with plant lifetime extension, approaching an asymptotic limit governed by OpEx. Taken together, these results emphasize that while energy price volatility dictates short-term operational competitiveness, design decisions that extend plant life and maximize equipment utilization are crucial for long-term cost and plant break-even minimization.

5. CONCLUSIONS

This work establishes a direct link between laboratory-scale PSA experiments, validated dynamic modeling, and industrial-scale techno-economic assessment for the capture of CO_2 from flue gas using MIL-160(Al). The shaped MOF exhibited favorable separation characteristics, with rinse flows improving CO_2 purity and purge flows primarily restoring capacity but penalizing both purity and productivity when overdosed. Scale-up simulations confirmed that optimal performance is achieved within a narrow interior operating window characterized by moderate rinse and minimized purge, consistent across laboratory and industrial domains. Techno-economic evaluation identified a total capital cost of \$18.89 M and an annualized CapEx of \$1.82 $M \cdot yr^{-1}$, with electricity consumption emerging as the dominant operating expense. Sensitivity analyses demonstrated that reducing the energy intensity yields the greatest economic gains, while adsorbent cost and durability improvements provide incremental benefits. Overall, this study provides a rigorous, experimentally anchored framework for bridging MOF-based adsorption studies to industrial CO_2 capture and underscores that material advances must be paired with process-level energy efficiency improvements to achieve cost-competitive deployment.

■ ASSOCIATED CONTENT

Supporting Information

The Supporting Information is available free of charge at https://pubs.acs.org/doi/10.1021/acs.iecr.5c04931.

> N_2 adsorption−desorption isotherm at 77 K; experimental details (breakthrough & PSA); techno-economic assessment (TEA); impact of purge flow rates on PSA experiments; and detailed description of the developed model (PDF)

■ AUTHOR INFORMATION

Corresponding Author

Mohsen Karimi − *Laboratory of Separation and Reaction Engineering (LSRE), Associate Laboratory LSRE/LCM, Faculty of Engineering and ALiCE - Associate Laboratory in Chemical Engineering, Faculty of Engineering, University of Porto, Porto 4200-465, Portugal;* orcid.org/0000-0002-1886-5454; Phone: +351 934 070 714; Email: mohsen.karimi@fe.up.pt

Authors

Mohammad Shirzad − *Laboratory of Separation and Reaction Engineering (LSRE), Associate Laboratory LSRE/LCM, Faculty of Engineering and ALiCE - Associate Laboratory in Chemical Engineering, Faculty of Engineering, University of Porto, Porto 4200-465, Portugal*

Rafael M. Siqueira − *Laboratory of Separation and Reaction Engineering (LSRE), Associate Laboratory LSRE/LCM, Faculty of Engineering and ALiCE - Associate Laboratory in Chemical Engineering, Faculty of Engineering, University of Porto, Porto 4200-465, Portugal; Laboratory of Adsorption and Catalysis, Department of Analytical and Physical Chemistry, Campus do Pici, Federal University of Ceara, Fortaleza-CE 60020-181, Brazil*

Alexandre Ferreira − *Laboratory of Separation and Reaction Engineering (LSRE), Associate Laboratory LSRE/LCM, Faculty of Engineering and ALiCE - Associate Laboratory in Chemical Engineering, Faculty of Engineering, University of Porto, Porto 4200-465, Portugal;* orcid.org/0000-0002-6746-8973

José A. C. Silva − *Centro de Investigação de Montanha (CIMO) and Laboratório Associado para a Sustentabilidade e Tecnologia em Regiões de Montanha (SusTEC), Instituto Politécnico de Bragança, Bragança 5300-253, Portugal;* orcid.org/0000-0003-1778-3833

Alírio E. Rodrigues − *Laboratory of Separation and Reaction Engineering (LSRE), Associate Laboratory LSRE/LCM, Faculty of Engineering and ALiCE - Associate Laboratory in Chemical Engineering, Faculty of Engineering, University of Porto, Porto 4200-465, Portugal;* orcid.org/0000-0002-0715-4761

Complete contact information is available at: https://pubs.acs.org/10.1021/acs.iecr.5c04931

Notes

The authors declare no competing financial interest.

■ ACKNOWLEDGMENTS

This work was supported by national funds through FCT/MCTES (PIDDAC): CIMO UID/00690/2025 (10.54499/UID/00690/2025) and UID/PRR/00690/2025 (10.54499/UID/PRR/00690/2025); SusTEC, LA/P/0007/2020 (DOI: 10.54499/LA/P/0007/2020). The authors also would like to acknowledge Christian Serre and Farid Nouar from Institut des Matériaux Poreux de Paris, ESPCI Paris, Ecole Normale Supérieure, PSL University, Paris, France, for providing the MOF MIL-160(Al) samples. They also recognize the scientific/industrial counseling provided by Padjam Polymer Development Co. (Private joint stock), Asaluyeh Port, Iran.

■ REFERENCES

(1) Slameršak, A.; Kallis, G.; O'Neill, D. W.; Hickel, J. Post-Growth: A Viable Path to Limiting Global Warming to 1.5°C. *One Earth* **2023**, 7..

(2) Shayesteh, H.; Sayari, A. Amine-Functionalized Lignin for CO2 Capture. 1: Phenolation- Enhanced Amine Grafting. *Sep. Purif. Technol.* **2026**, 380, 135502.

(3) Vitillo, J. G.; Eisaman, M. D.; Aradóttir, E. S. P.; Passarini, F.; Wang, T.; Sheehan, S. W. The Role of Carbon Capture, Utilization, and Storage for Economic Pathways That Limit Global Warming to below 1.5°C. *iScience* **2022**, *25* (5), 104237.

(4) Figueroa, J. D.; Fout, T.; Plasynski, S.; McIlvried, H.; Srivastava, R. D. Advances in CO2 Capture Technology—The U.S. Department of

Energy's Carbon Sequestration Program. *Int. J. Greenh. Gas Control* **2008**, 2 (1), 9−20.

(5) IPCC *Climate Change 2022: Impacts, Adaptation and Vulnerability. Contribution of Working Group II to the Sixth Assessment Report of the Intergovernmental Panel on Climate Change*; Cambridge University Press: Cambridge, UK and New York, NY, USA, 2022; p 3056.

(6) D'Alessandro, D.; Smit, B.; Long, J. R. Carbon Dioxide Capture: Prospects for New Materials. *Angew. Chem., Int. Ed.* **2010**, *49* (35), 6058−6082.

(7) Citaristi, I. International Energy Agency (IEA). In *The Europa directory of international organizations 2022*; Routledge, 2022; .

(8) Mac Dowell, N.; Fennell, P. S.; Shah, N.; Maitland, G. C. The Role of CO2 Capture and Utilization in Mitigating Climate Change. *Nat. Clim. Chang.* **2017**, *7* (4), 243−249.

(9) Kearns, D. Technology Readiness and Costs of CCS. *Global CCS Institute* **2021**, *3*.

(10) Dods, M. N.; Kim, E. J.; Long, R., J.; Weston, C.; Deep CCS, S. Moving Beyond 90% Carbon Dioxide Capture. *Environ. Sci. Technol.* **2021**, *55* (13), 8524−8534.

(11) *Electric Power Research Institute, Program on Technology Innovation: Post-Combustion CO2 Capture Technology Development*; Electric Power Research Institute, Palo Alto, 2008.

(12) Karimi, M.; Shirzad, M.; Silva, J. A. C.; Rodrigues, A. E. Carbon Dioxide Separation and Capture by Adsorption: A Review. *Environ. Chem. Lett.* **2023**, *21*, 2041−2084.

(13) Safarzadeh Khosrowshahi, M.; Afshari Aghajari, A.; Rahimi, M.; Maleki, F.; Ghiyabi, E.; Rezanezhad, A.; Bakhshi, A.; Salari, E.; Shayesteh, H.; Mohammadi, H. Recent Progress on Advanced Solid Adsorbents for CO2 Capture: From Mechanism to Machine Learning. *Mater. Today Sustain.* **2024**, *27*, 100900.

(14) Ding, M.; Flaig, R. W.; Jiang, H. L.; Yaghi, O. M. Carbon Capture and Conversion Using Metal−Organic Frameworks and MOF-Based Materials. *Chem. Soc. Rev.* **2019**, *48* (10), 2783−2828.

(15) Karimi, M.; Ferreira, A.; Rodrigues, A. E.; Nouar, F.; Serre, C.; Silva, J. A. C. MIL-160(Al) as a Candidate for Biogas Upgrading and CO2 Capture by Adsorption Processes. *Ind. Eng. Chem. Res.* **2023**, *62* (12), 5216−5229.

(16) Burtch, N. C.; Jasuja, H.; Walton, K. S. Water Stability and Adsorption in Metal-Organic Frameworks. *Chem. Rev.* **2014**, *114* (20), 10575−10612.

(17) Brandt, P.; Nuhnen, A.; Lange, M.; Möllmer, J.; Weingart, O.; Janiak, C. Metal-Organic Frameworks with Potential Application for SO2 Separation and Flue Gas Desulfurization. *ACS Appl. Mater. Interfaces* **2019**, *11* (19), 17350−17358.

(18) Younas, M.; Rezakazemi, M.; Daud, M.; Wazir, M. B.; Ahmad, S.; Ullah, N.; Inamuddin Ramakrishna, S. Recent Progress and Remaining Challenges in Post-Combustion CO2 Capture Using Metal-Organic Frameworks (MOFs). *Prog. Energy Combust. Sci.* **2020**, *80*, 100849.

(19) Taddei, M.; Petit, C. Engineering Metal−Organic Frameworks for Adsorption-Based Gas Separations: From Process to Atomic Scale. *Mol. Syst. Des. Eng.* **2021**, *6* (11), 841−875.

(20) Nguyen, T. T. T.; Shimizu, G. K. H.; Rajendran, A. CO2/N2 Separation by Vacuum Swing Adsorption Using a Metal−Organic Framework, CALF-20: Multi-Objective Optimization and Experimental Validation. *Chem. Eng. J.* **2023**, *452*, 139550.

(21) Karimi, M.; Siqueira, R. M.; Rodrigues, A. E.; Nouar, F.; Silva, J. A. C.; Serre, C.; Ferreira, A. Biogas Upgrading Using Shaped MOF MIL-160(Al) by Pressure Swing Adsorption Process: Experimental and Dynamic Modelling Assessment. *Sep. Purif. Technol.* **2024**, *344*, 127260.

(22) Karimi, M.; Shirzad, M.; Silva, J. A. C.; Rodrigues, A. E. Biomass/Biochar Carbon Materials for CO2 Capture and Sequestration by Cyclic Adsorption Processes: A Review and Prospects for Future Directions. *J. CO_2 Util.* **2022**, *57*, 101890.

(23) Nikolaidis, G. N.; Kikkinides, E. S.; Georgiadis, M. C. An Integrated Two-Stage P/VSA Process for Postcombustion CO2 Capture Using Combinations of Adsorbents Zeolite 13X and Mg-MOF-74. *Ind. Eng. Chem. Res.* **2017**, *56* (4), 974−988.

(24) Ye, S.; Jiang, X.; Ruan, L. W.; Liu, B.; Wang, Y. M.; Zhu, J. F.; Qiu, L. G. Post-Combustion CO2 Capture with the HKUST-1 and MIL-101(Cr) Metal−Organic Frameworks: Adsorption, Separation and Regeneration Investigations. *Microporous Mesoporous Mater.* **2013**, *179*, 191−197.

(25) Ben-Mansour, R.; Bamidele, O. E.; Habib, M. A. Evaluation of Mg-MOF-74 for Post-Combustion Carbon Dioxide Capture through Pressure Swing Adsorption. *Int. J. Energy Res.* **2015**, *39* (15), 1994−2007.

(26) Nguyen, T. T. T.; Lin, J. B.; Shimizu, G. K. H.; Rajendran, A. Separation of CO2 and N2 on a Hydrophobic Metal Organic Framework CALF-20. *Chem. Eng. J.* **2022**, *442*, 136263.

(27) Chen, B.; Fan, D.; Pinto, R. V.; Dovgaliuk, I.; Nandi, S.; Chakraborty, D.; García-Moncada, N.; Vimont, A.; McMonagle, C. J.; Bordonhos, M.; Al Mohtar, A.; Cornu, I.; Florian, P.; Heymans, N.; Daturi, M.; De Weireld, G.; Pinto, M.; Nouar, F.; Maurin, G.; Mouchaham, G.; Serre, C. A. Scalable Robust Microporous Al-MOF for Post-Combustion Carbon Capture. *Adv. Sci.* **2024**, *11*, 2401070.

(28) Loughran, R. P.; Hurley, T.; Gładysiak, A.; Chidambaram, A.; Khivantsev, K.; Walter, E. D.; Graham, T. R.; Reardon, P.; Szanyi, J.; Fast, D. B.; Miller, Q. R. S.; Park, A. H. A.; Stylianou, K. C. CO2 Capture from Wet Flue Gas Using a Water-Stable and Cost-Effective Metal-Organic Framework. *Cell Rep. Phys. Sci.* **2023**, *4* (7), 101470.

(29) Perbet, M.; Michon, T.; Quadrelli, E. A.; Bonneau, M.; Farrusseng, D. Scalable One-Step Syntheses of Aluminium-Based MOFs. *Chem. Commun.* **2025**, *61* (67), 12562−12565.

(30) Permyakova, A.; Skrylnyk, O.; Courbon, E.; Affram, M.; Wang, S.; Lee, U. H.; Valekar, A. H.; Nouar, F.; Mouchaham, G.; Devic, T.; De Weireld, G.; Chang, J. S.; Steunou, N.; Frère, M.; Serre, C. Synthesis Optimization, Shaping, and Heat Reallocation Evaluation of the Hydrophilic Metal−Organic Framework MIL-160(Al). *ChemSusChem* **2017**, *10* (7), 1419−1426.

(31) Karimi, M.; Janiak, C. The Metal−Organic Framework MIL-160: Comprehensive Insights into Synthesis and Applications. *Chem. Commun.* **2025**, *61* (95), 18742−18755.

(32) Severino, M. I.; Gkaniatsou, E.; Nouar, F.; Pinto, M. L.; Serre, C. MOFs Industrialization: A Complete Assessment of Production Costs. *Faraday Discuss.* **2021**, *231* (0), 326−341.

(33) Ahn, H.; Luberti, M.; Liu, Z.; Brandani, S. Lab-Scale Pilot for CO2 Capture Vacuum Pressure Swing Adsorption: MIL-160(Al) vs Zeolite 13X. *Carbon Capture Sci. Technol.* **2024**, *12*, 100224.

(34) Danaci, D.; Webley, P. A.; Petit, C. Guidelines for Techno-Economic Analysis of Adsorption Processes. *Front. Chem. Eng.* **2021**, *2*, 602430.

(35) Karimi, M.; Siqueira, R. M.; Shirzad, M.; Ferreira, A. F. P.; Rodrigues, A. E.; Silva, J. A. C. Integrated Experimental, Process Simulation, and Techno-Economic Assessment of Biogas Upgrading via Pressure/Vacuum Swing Adsorption. *Sep. Purif. Technol.* **2026**, *386*, 136571.

(36) Karimi, M.; Shirzad, M. Sustainable Industrial Process Design for Derived CO2 Adsorbent from Municipal Solid Wastes: Scale-up, Techno-Economic and Parametric Assessment. *Sustain. Mater. Technol.* **2024**, *41*, No. e01091.

(37) Smith, R. *Chemical Process Design and Integration*, 2nd ed.; Wiley: NJ, 2016.

(38) Do, D. D. *Adsorption Analysis: Equilibria and Kinetics (With CD Containing Computer Matlab Programs)*, 1st ed.; World Scientific: London, 1998; Vol. *2*.

(39) Karimi, M.; Rodrigues, A. E.; Silva, J. A. C. Designing a Simple Volumetric Apparatus for Measuring Gas Adsorption Equilibria and Kinetics of Sorption. Application and Validation for CO2, CH4 and N2 Adsorption in Binder-Free Beads of 4A Zeolite. *Chem. Eng. J.* **2021**, *425*, 130538.

(40) Ruthven, D. M. *Principles of Adsorption and Adsorption Processes*, 1st ed.; Wiley: New York, 1984.

(41) Karimi, M.; Aly, E.; Rodrigues, A. E.; Da Silva Freitas, F. A.; Silva, J. A. C. Experimental and Dynamic Modeling Study of CO2/N2 Separation on Ion-Exchanged Binder-Free LTA Zeolites for Post-Combustion Carbon Capture. *Sep. Purif. Technol.* **2026**, *391* (23), 137050.

(42) Ribeiro, A. M.; Santos, J. C.; Rodrigues, A. E. Pressure Swing Adsorption for CO2 Capture in Fischer−Tropsch Fuels Production from Biomass. *Adsorption* **2011**, *17* (3), 443−452.

(43) Gebremariam, S. K.; Al Wahedi, Y.; AlHajaj, A.; Dumée, L. F.; Karanikolos, G. N. System-Level Comparison and Techno-Economic Evaluation of Structured Metal−Organic Framework Adsorbents for Post-Combustion CO2 Capture by Vacuum/Pressure Swing Adsorption. *Chem. Eng. J.* **2025**, *505*, 159384.

(44) Jung, W.; Lee, J. Economic Evaluation for Four Different Solid Sorbent Processes with Heat Integration for Energy-Efficient CO2 Capture Based on PEI-Silica Sorbent. *Energy* **2022**, *238*, 121864.

(45) Balogun, H. A.; Bahamon, D.; Almenhali, S.; Vega, L. F.; Alhajaj, A. Are We Missing Something When Evaluating Adsorbents for CO2 Capture at the System Level? *Energy Environ. Sci.* **2021**, *14* (12), 6360−6380.

(46) James, I. R. E.; Zoelle, A.; Keairns, D.; Turner, M.; Woods, M.; Kuehn, N. *Cost and Performance Baseline for Fossil Energy Plants Vol. 1*; Bituminous Coal and Natural Gas to Electricity, 2019.

(47) Charalambous, C.; Moubarak, E.; Schilling, J.; Sanchez Fernandez, E.; Wang, J. Y.; Herraiz, L.; Mcilwaine, F.; Peh, S. B.; Garvin, M.; Jablonka, K. M.; Moosavi, S. M.; Van Herck, J.; Ozturk, A. Y.; Pourghaderi, A.; Song, A. Y.; Mouchaham, G.; Serre, C.; Reimer, J. A.; Bardow, A.; Smit, B.; Garcia, S. A Holistic Platform for Accelerating Sorbent-Based Carbon Capture. *Nature* **2024**, *632* (8023), 89−94.

(48) Gardarsdottir, S. O.; De Lena, E.; Romano, M.; Roussanaly, S.; Voldsund, M.; Pérez-Calvo, J. F.; Berstad, D.; Fu, C.; Anantharaman, R.; Sutter, D.; Gazzani, M.; Mazzotti, M.; Cinti, G. Comparison of Technologies for CO2 Capture from Cement Production—Part 2: Cost Analysis. *Energies* **2019**, *12* (3), 12.

(49) Tingelinhas, J.; Saragoça, C.; Al Mohtar, A.; Mateus, M.; Pinto, M. L. Pillared Clays as Cost-Effective Adsorbents for Carbon Capture by Pressure Swing Adsorption Processes in the Cement Industry. *Ind. Eng. Chem. Res.* **2023**, *62* (13), 5613−5623.